

# Simultaneous acquisition of 3D shape and deformation by combination of interferometric and correlation-based laser speckle metrology

Markus Dekiff,<sup>1,\*</sup> Philipp Berssenbrügge,<sup>1</sup> Björn Kemper,<sup>2</sup> Cornelia Denz,<sup>3</sup>  
and Dieter Dirksen<sup>1</sup>

<sup>1</sup>Department of Prosthetic Dentistry and Biomaterials, University of Münster, Waldeyerstraße 30, 48149 Münster, Germany

<sup>2</sup>Biomedical Technology Center of the Medical Faculty, University of Münster, Mendelstraße 17, 48129 Münster, Germany

<sup>3</sup>Institute of Applied Physics, University of Münster, Corrensstraße 2, 48149 Münster, Germany  
\*markus.dekiff@uni-muenster.de

**Abstract:** A metrology system combining three laser speckle measurement techniques for simultaneous determination of 3D shape and micro- and macroscopic deformations is presented. While microscopic deformations are determined by a combination of Digital Holographic Interferometry (DHI) and Digital Speckle Photography (DSP), macroscopic 3D shape, position and deformation are retrieved by photogrammetry based on digital image correlation of a projected laser speckle pattern. The photogrammetrically obtained data extend the measurement range of the DHI-DSP system and also increase the accuracy of the calculation of the sensitivity vector. Furthermore, a precise assignment of microscopic displacements to the object's macroscopic shape for enhanced visualization is achieved. The approach allows for fast measurements with a simple setup. Key parameters of the system are optimized, and its precision and measurement range are demonstrated. As application examples, the deformation of a mandible model and the shrinkage of dental impression material are measured.

©2015 Optical Society of America

**OCIS codes:** (120.0120) Instrumentation, measurement, and metrology; (030.6140) Speckle; (120.2880) Holographic interferometry; (120.4290) Nondestructive testing; (150.0150) Machine vision; (100.0100) Image processing.

## References and links

1. T. Kreis, *Handbook of Holographic Interferometry: Optical and Digital Methods* (Wiley VCH, 2004).
2. H. J. Tiziani and G. Pedrini, "From speckle pattern photography to digital holographic interferometry [Invited]," *Appl. Opt.* **52**(1), 30–44 (2013).
3. M. Sjö Dahl, "Some recent advances in electronic speckle photography," *Opt. Lasers Eng.* **29**(2–3), 125–144 (1998).
4. T. Fricke-Begemann and J. Burke, "Speckle interferometry: three-dimensional deformation field measurement with a single interferogram," *Appl. Opt.* **40**(28), 5011–5022 (2001).
5. D. Dirksen, J. Gettkant, G. Bischoff, B. Kemper, Z. Böröcz, and G. von Bally, "Improved evaluation of electronic speckle pattern interferograms by photogrammetric image analysis," *Opt. Lasers Eng.* **44**(5), 443–454 (2006).
6. H. Babovsky, M. Hanemann, M. Große, A. Kießling, and R. Kowarschik, "Stereophotogrammetric Image Field Holography," in *Fringe 2013*, W. Osten, ed. (Springer Berlin Heidelberg, 2014), pp. 875–878.
7. W. Osten, "Application of optical shape measurement for the nondestructive evaluation of complex objects," *Opt. Eng.* **39**(1), 232–243 (2000).
8. M. Dekiff, P. Berssenbrügge, B. Kemper, C. Denz, and D. Dirksen, "Three-dimensional data acquisition by digital correlation of projected speckle patterns," *Appl. Phys. B.* **99**(3), 449–456 (2010).
9. P. Berssenbrügge, M. Dekiff, B. Kemper, C. Denz, and D. Dirksen, "Characterization of the 3D resolution of topometric sensors based on fringe and speckle pattern projection by a 3D transfer function," *Opt. Lasers Eng.* **50**(3), 465–472 (2012).

10. H. Babovsky, M. Grosse, J. Buehl, A. Kiessling, and R. Kowarschik, "Stereophotogrammetric 3D shape measurement by holographic methods using structured speckle illumination combined with interferometry," *Opt. Lett.* **36**(23), 4512–4514 (2011).
11. R. Schwede, H. Babovsky, A. Kiessling, and R. Kowarschik, "Measurement of three-dimensional deformation vectors with digital holography and stereophotogrammetry," *Opt. Lett.* **37**(11), 1943–1945 (2012).
12. M. Schaffer, M. Große, B. Harendt, and R. Kowarschik, "Coherent two-beam interference fringe projection for highspeed three-dimensional shape measurements," *Appl. Opt.* **52**(11), 2306–2311 (2013).
13. I. Yamaguchi and T. Zhang, "Phase-shifting digital holography," *Opt. Lett.* **22**(16), 1268–1270 (1997).
14. I. Yamaguchi, T. Ida, M. Yokota, and K. Yamashita, "Surface shape measurement by phase-shifting digital holography with a wavelength shift," *Appl. Opt.* **45**(29), 7610–7616 (2006).
15. J.-P. Liu and T.-C. Poon, "Two-step-only quadrature phase-shifting digital holography," *Opt. Lett.* **34**(3), 250–252 (2009).
16. V. Bianco, M. Paturzo, and P. Ferraro, "Spatio-temporal scanning modality for synthesizing interferograms and digital holograms," *Opt. Express* **22**(19), 22328–22339 (2014).
17. J. Goodman, *Speckle Phenomena in Optics* (Roberts and Company Publishers, 2010).
18. M. Takeda, H. Ina, and S. Kobayashi, "Fourier-transform method of fringe-pattern analysis for computer-based topography and interferometry," *J. Opt. Soc. Am.* **72**(1), 156–160 (1982).
19. H. A. Aebischer and S. Waldner, "A simple and effective method for filtering speckle-interferometric phase fringe patterns," *Opt. Commun.* **162**(4–6), 205–210 (1999).
20. M. A. Herráez, D. R. Burton, M. J. Lalor, and M. A. Gdeisat, "Fast two-dimensional phase-unwrapping algorithm based on sorting by reliability following a noncontinuous path," *Appl. Opt.* **41**(35), 7437–7444 (2002).
21. M. Sjö Dahl and L. R. Benckert, "Electronic speckle photography: analysis of an algorithm giving the displacement with subpixel accuracy," *Appl. Opt.* **32**(13), 2278–2284 (1993).
22. O. Faugeras, *Three-Dimensional Computer Vision* (The MIT Press, 1993).
23. R. Hartley and A. Zisserman, *Multiple View Geometry in Computer Vision* (Cambridge University Press, 2004).
24. H. Lu and P. D. Cary, "Deformation measurements by digital image correlation: Implementation of a second-order displacement gradient," *Exp. Mech.* **40**(4), 393–400 (2000).
25. A. Fusiello, E. Trucco, and A. Verri, "A compact algorithm for rectification of stereo pairs," *Mach. Vis. Appl.* **12**(1), 16–22 (2000).
26. W. H. Press, S. A. Teukolsky, W. T. Vetterling, and B. P. Flannery, *Numerical Recipes 3rd Edition: The Art of Scientific Computing* (Cambridge University Press, 2007).
27. Z. Zhang, "A flexible new technique for camera calibration," *IEEE Trans. Pattern Anal. Mach. Intell.* **22**(11), 1330–1334 (2000).
28. G. Bradski, "The OpenCV Library," *Dr Dobb's J. Softw. Tools* (2000).
29. S. Bochkhanov, "ALGLIB," <http://www.alglib.net>.
30. M. Frigo and S. G. Johnson, "The Design and Implementation of FFTW3," *Proc. IEEE* **93**(2), 216–231 (2005).
31. C. Remmersmann, S. Stürwald, B. Kemper, P. Langehanenberg, and G. von Bally, "Phase noise optimization in temporal phase-shifting digital holography with partial coherence light sources and its application in quantitative cell imaging," *Appl. Opt.* **48**(8), 1463–1472 (2009).
32. R. C. Gonzalez and R. E. Woods, *Digital Image Processing* (Prentice Hall, 2007).
33. N.-E. Molin, M. Sjö Dahl, P. Gren, and A. Svanbro, "Speckle photography combined with speckle interferometry," *Opt. Lasers Eng.* **41**(4), 673–686 (2004).
34. A. Andersson, A. Runnemalm, and M. Sjö Dahl, "Digital Speckle-Pattern Interferometry: Fringe Retrieval for Large In-Plane Deformations With Digital Speckle Photography," *Appl. Opt.* **38**(25), 5408–5412 (1999).

## 1. Introduction

Digital Holographic Interferometry (DHI) is a well-established method for the precise measurement of microscopic deformations [1,2]. By employing DHI for the retrieval of the out-of-plane deformation component and combining it with Digital Speckle Photography (DSP) [3] for the measurement of the in-plane deformation components, 3D deformation fields can be acquired from a single pair of holograms with a simple experimental setup [4].

We combine this technique with a photogrammetric method that allows the acquisition of the macroscopic three-dimensional shape of the object's surface. The 3D shape data is used for an accurate calculation of the sensitivity vector, which is necessary for the conversion of phase data acquired by DHI into deformation values. Furthermore, the shape measurement can be used to detect deformations exceeding the measurement ranges of DHI and DSP. Another benefit of the combination of these techniques is the possibility to precisely assign deformation data to the macroscopic shape of the object for visualization purposes.

The combination of Electronic Speckle Pattern Interferometry (ESPI) [2], which is closely related to DHI, with a photogrammetric 3D coordinate measurement technique has been reported previously by Dirksen et al. [5]. However, the former approach required a manual analysis of corresponding points for 3D data acquisition and thus did not allow true full-field measurements. Approaches employing the fringe projection technique for 3D shape retrieval

[6,7] require an additional device for structured illumination. On the other hand, the acquisition of 3D data by automated correlation of a projected laser speckle pattern [8,9] can utilize the same laser that is used for DHI and DSP. Furthermore, it is possible to employ this technique also simultaneously with DHI and DSP. While other recently introduced techniques for fast 3D data acquisition using laser-light patterns [10–12] offer a higher spatial resolution, our approach needs only a single stereo image instead of an image sequence, thus allowing higher temporal resolution.

The employed DHI technique [4] uses an off-axis configuration. For each state of the object only a single (spatially phase-biased) hologram has to be recorded. In comparison with (temporal) phase-shifting digital holography [13–15], the temporal resolution is higher and the stability requirements are lower. Furthermore, the experimental setup is simpler because no device for shifting the phase of the reference wave (or for shifting the object [16]) is needed.

As all three combined methods require only a single shot of the object during the deformation process and can be applied simultaneously, short measurement times can be achieved.

After a description of the basics of the combined techniques and their implementation, we investigate the influence of various parameters of the measurement system, e.g., the size of the projected speckles and the sizes of the apertures in front of the cameras, on the achieved measurement range and precision. The demands of the combined three speckle metrology techniques are to some extent contradictory and depend on the deformations to be measured. Hence, optimum parameter sets with regard to the expected deformations are discussed. Finally, we demonstrate the applicability of our approach by measuring the 3D deformation of a mandible model due to mechanical loading of an inserted dental implant.

## 2. Experimental methods

### 2.1 Speckle effect

The scattering of coherent light induced by a rough surface or in a medium with varying refractive index results in a spatially modulated intensity distribution that is called a speckle field [17]. If this primary speckle field is reflected by another rough surface, a secondary speckle field is generated, whose amplitudes are modulated by the primary (initial) speckle field. Our approach makes use of both these fields: The automated photogrammetric 3D shape acquisition evaluates the “objective” speckle pattern that is formed on the investigated surface by the primary speckle field. In DHI and DSP “subjective” speckle patterns are evaluated, i.e., speckle patterns that are formed in the image plane, when a surface illuminated by coherent light is imaged. For measurements using all 3 techniques simultaneously the investigated surface is illuminated by a primary speckle field. In this case the analyzed subjective speckle pattern corresponds to the imaged secondary speckle field.

### 2.2 Digital holographic interferometry

Digital Holographic Interferometry is a well-proven method for the contactless determination of microscopic deformations for non-destructive material analyses [1,2]. In the presented approach, image plane DHI is used to determine deformations in direction of the optical axis of the measurement system (out-of-plane).

The illumination of the object by the expanded object beam leads to a speckle pattern that is imaged onto a digital sensor where it is superimposed with the (expanded) reference wave field to form a hologram (Fig. 1).

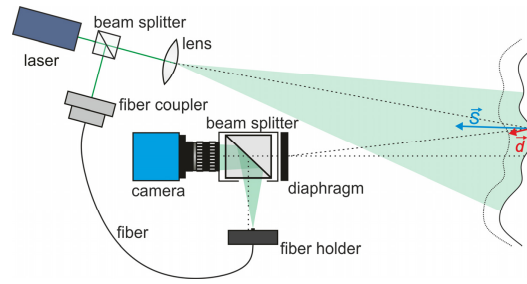


Fig. 1. Experimental setup for image plane digital holography including sensitivity vector  $\vec{S}$  and deformation vector  $\vec{d}$ .

One hologram is recorded before and one after the deformation. The pair of holograms is then evaluated in order to determine the change of the object waves' (i.e., the light scattered by the object) phase distribution, which permits conclusions about the underlying deformation.

We employ the Fourier transform method [18] (following the approach described in [4]) to retrieve the object wave's phase and intensity distributions (the latter is required for DSP). The necessary spatial phase gradient between object and reference wave is achieved by an offset of the reference wave from the optical axis.

To reconstruct the object wave front from a hologram, first its discrete Fourier transform (DFT) is calculated (Fig. 2(a)). Then one of the sidebands is isolated using an 11-sided polygon with smoothed edges as frequency filter function (Fig. 2(b)) and shifted to the origin of the frequency space. Calculating the inverse DFT yields the complex amplitude of the object wave from which phase and intensity distribution are available.

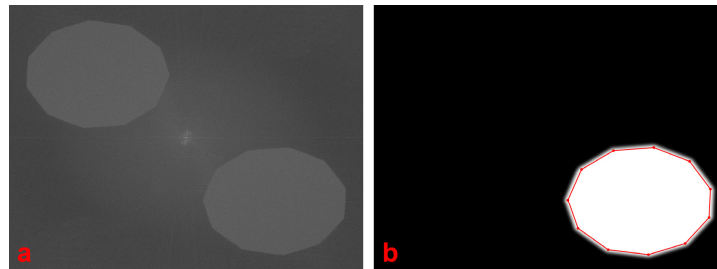


Fig. 2. Fourier transform of a hologram in logarithmic scale (a) and filter function (b) with the sideband's border (red).

In practice, the sidebands usually overlap with the speckle halo, i.e., the spectrum of the object wave's intensity distribution, and the spectrum of the reference wave (if it does not illuminate the sensor uniformly). This leads to a systematic error in the reconstruction of the object wave. To eliminate the spectrum of the reference wave, its intensity distribution is recorded separately before each measurement series and subtracted from the holograms. This is not possible for the intensity distribution of the object wave as it changes during the measurement. Hence, the reconstruction of the object wave is performed iteratively. In each iteration step the object wave's intensity distribution calculated in the previous step is subtracted from the original hologram.

When the phase distributions corresponding to the initial and deformed state have been determined, the difference between them is calculated. The resulting phase difference distribution (Fig. 3(a)) is wrapped modulo  $2\pi$ . After being filtered with a sine-cosine filter that reduces noise while preserving the  $2\pi$  discontinuities [19], its continuous form (Fig. 3(b)) is retrieved by phase unwrapping using the algorithm described in [20].

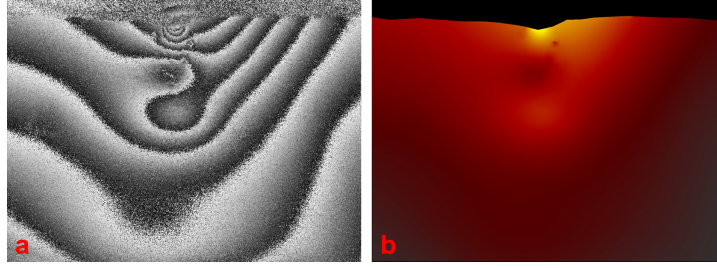


Fig. 3. Phase difference distribution modulo  $2\pi$  (a) and unwrapped (b).

Then the underlying deformation  $\vec{d}(x, y, z)$  can be calculated using the relationship:

$$\Delta\phi(x, y, z) = \frac{2\pi}{\lambda} \vec{d}(x, y, z) \cdot \vec{S}(x, y, z), \quad (1)$$

where  $\Delta\phi$  represents the unwrapped phase map and  $\lambda$  constitutes the wavelength. The sensitivity vector  $\vec{S}(x, y, z)$ , i.e., the sum of the unit vectors in observation and illumination direction (Fig. 1), considers the imaging geometry of the measurement system. If the geometry of the experimental setup is chosen in such a way that the sensitivity of the interferometer focuses mainly in direction of the optical axis ( $z$ -axis), and if the in-plane deformations are small, we get:

$$d_z(x, y, z) \approx \frac{\lambda}{2\pi} \frac{\Delta\phi(x, y, z)}{S_z(x, y, z)}. \quad (2)$$

Particularly in case of larger in-plane deformations, the results for  $d_x$  and  $d_y$  obtained by DSP can be used to solve Eq. (1) for  $d_z$  more accurately.

### 2.3 Digital speckle photography

Digital Speckle Photography [3] is applied to determine surface displacements perpendicular to the optical axis of the measurement system. When a diffusely reflecting surface is illuminated by coherent laser light, a lateral shift of the surface causes a proportional lateral shift of the generated speckle pattern. This relation can be used to determine lateral displacements of surface regions by quantifying the lateral shift of the corresponding regions in images of the speckle patterns before and after deformation/translation of the object.

For this purpose, Digital Image Correlation (DIC) [21] is employed: the speckle image of the initial object state is defined as reference image and divided into small square regions (sub-images). These sub-images are then searched for in the so-called search image, i.e., the image of the deformed state. This is done by comparing the sub-image of the reference image to different sub-images of the search image, calculating the similarity for each combination and, finally, by identifying the sub-image of the search image that yields the highest similarity value. In our case the similarity is quantified by the two-dimensional cross-correlation coefficient [21]

$$C = \sum_{k=-\frac{m-1}{2}}^{\frac{m-1}{2}} \sum_{l=-\frac{m-1}{2}}^{\frac{m-1}{2}} [f_1(u_0 + k, v_0 + l) f_2(u_0 + k + U_0, v_0 + l + V_0)]. \quad (3)$$

Here,  $m$  is the (odd) width and height of the sub-images,  $f_1$  and  $f_2$  represent the intensity distributions of the reference and search image, respectively,  $u_0$  and  $v_0$  are the pixel coordinates of the center point of the sub-image in the reference image,  $u_0 + U_0$  and  $v_0 + V_0$  denote the pixel coordinates of the center of a sub-image in the search image.

Those values for  $U_0$  and  $V_0$  that maximize  $C$  (Fig. 4) state the average displacement of the central point of the sub-image in pixel lengths, which can be converted to metric lengths using the calibrated imaging scale.

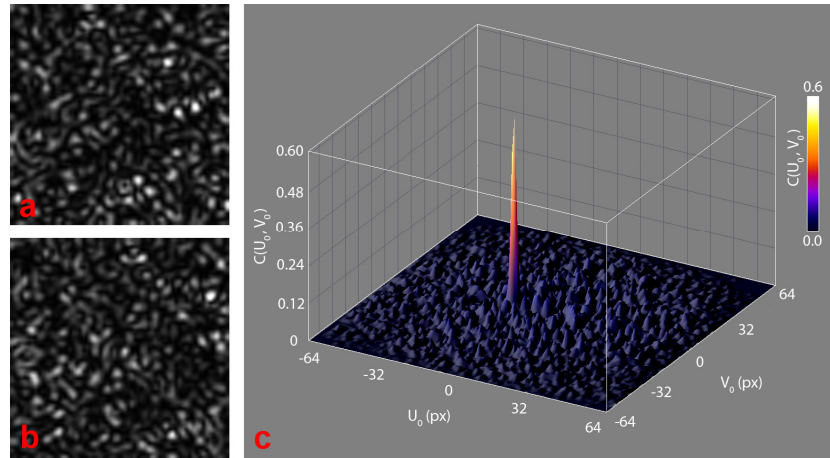


Fig. 4. Sub-images at the same image position before (a) and after (b) a displacement of the observed surface as well as the correlation function  $C(U_0, V_0)$  (c).

In order to evaluate Eq. (3) more efficiently the calculations are carried out in the spectral domain. Sub-pixel accuracy is achieved by determining the maximum of the estimated continuous correlation function that is obtained by a Fourier series expansion of the peak of the discrete correlation function  $C(U_0, V_0)$  [21].

As described in the previous section, for simultaneous measurements with DHI and DSP the speckle pattern, i.e., the intensity of the object wave, can be reconstructed from the recorded hologram using the Fourier-transform method.

#### 2.4 3D shape acquisition by correlation of a projected speckle pattern

The macroscopic shape and position of the object are determined by stereophotogrammetry, a measurement technique that allows the determination of 3D coordinates from at least two images captured from different positions [22,23]. A crucial step in the evaluation process is the identification of common or corresponding points in the images. Our approach to automate this task is to illuminate the object with a speckle pattern (generated by a laser beam that passes a ground glass diffuser), recording an image pair with two digital cameras and using digital image correlation (see previous sect.) to identify corresponding image points. The centers of matching sub-images are considered as corresponding image points.

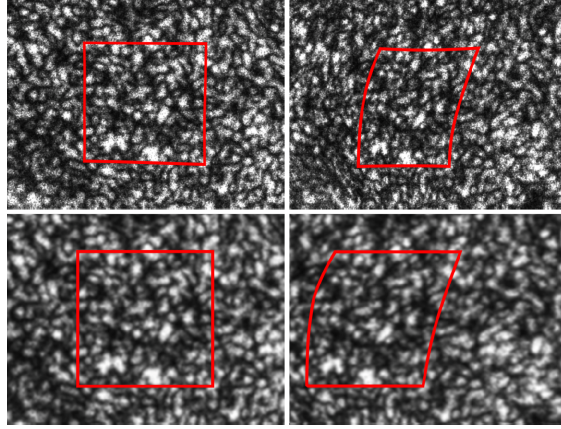


Fig. 5. Corresponding image regions in the original left and right camera images (top) and in the rectified and smoothed ones (bottom).

As corresponding image regions might differ considerably due to the differences of perspectives (Fig. 5), a DIC algorithm based on the algorithm proposed by Lu and Cary [24] is used, which takes larger geometric distortions of the sub-images into account. In order to simplify the correspondence analysis the image pair is rectified [25] prior to application of the DIC algorithm in such a way that corresponding image points are located in the same image row (Fig. 5). Thus, only distortions in one direction (here: horizontal) have to be considered. Interfering “subjective” speckle patterns are eliminated from the images with a Gaussian filter (kernel size: 5 x 5 pixels). In order to quantify the similarity between two sub-images, we use a sum of squared differences correlation coefficient that takes on its minimum value when the maximum similarity between sub-images is reached:

$$C = \frac{\sum_{k=-\frac{m-1}{2}}^{\frac{m-1}{2}} \sum_{l=-\frac{m-1}{2}}^{\frac{m-1}{2}} \left[ f(u_0 + k, v_0 + l) - \left[ g(u_0 + k + \Delta u, v_0 + l) - W \right] \right]^2}{\left[ \sum_{k=-\frac{m-1}{2}}^{\frac{m-1}{2}} \sum_{l=-\frac{m-1}{2}}^{\frac{m-1}{2}} \left[ f(u_0 + k, v_0 + l) \right] \right]^2}. \quad (4)$$

In Eq. (4),  $f(u, v)$  and  $g(u, v)$  represent the discrete gray level distributions of the images recorded by the first/left and second/right camera respectively,  $m$  is the (odd) width of the subsets. The parameters  $u_0$  and  $v_0$  are the pixel coordinates of the center point of the sub-image in the left image, while  $W$  represents an intensity offset between the sub-image in the left image and the corresponding region in the right image and  $\Delta u$  is calculated by

$$\Delta u = U_0 + U_u k + U_v l + \frac{1}{2} U_{uu} k^2 + \frac{1}{2} U_{vv} l^2 + U_{uv} kl. \quad (5)$$

$U_0$  describes the horizontal displacement of the sub-image center, thus leading to the desired point  $(u_0 + U_0, v_0)$  in the right image.  $U_u$ ,  $U_v$  and  $U_{uu}$ ,  $U_{vv}$ ,  $U_{uv}$  are the components of the first- and second-order displacement gradients, resp.

The minimization of  $C$  is handled as non-linear least-squares problem using the iterative Levenberg-Marquardt algorithm [26]. The starting values are obtained by calculating  $C$  for a series of values for  $U_0$  and  $U_u$  (usually the parameters with the highest absolute values) with all other parameters set to zero and finding the set that yields the lowest value for  $C$ .

The occurrence of false point correspondences is minimized by employing a threshold for  $C$  and checking for violations of the ordering constraint [22], i.e., if points in a row of the left (rectified) image are ordered the same way as their correspondences in the right (rectified) image. Furthermore, for each point the median of the  $U_0$  values of its 5 x 5 point environment is determined. The point is removed if the difference between its  $U_0$  and the median is larger than double the average difference between the median and the  $U_0$  values in the 5 x 5 point

environment. Points with less than 9 neighbors in the 5 x 5 vicinity are also removed. Finally, the coordinates of the 3D points belonging to valid correspondences are calculated.

### 2.5 Experimental setup

The experimental setup (Fig. 6) comprises an image plane DHI setup for out-of-plane measurements with a modified illumination component and two additional cameras.

A frequency doubled Nd:YAG cw laser with a wavelength of 532 nm and a power of 150 mW (Compass 315M-150, Coherent, Santa Clara, CA, USA) serves as light source. A combination of a rotatable half-wave plate and a polarizing beam splitter is employed to variably divide the laser light into an object and a reference beam. The object beam is focused on a ground glass to generate a speckle pattern that is used to illuminate the device under test. The average size of the projected speckles can be adjusted by changing the distance between ground glass and lens L2, which alters the illuminated area of the ground glass. The reference beam is coupled into a single-mode fiber. The light scattered back from the object, i.e., the object wave, is imaged onto the sensor of a monochrome CCD camera (C3) with a spatial resolution of 1600 x 1200 pixels and 256 gray levels (DMK 51BU02, The Imaging Source, Bremen, Germany) equipped with a 75 mm C-Mount lens (23FM75L, Tamron, Saitama, Japan; f-number: 3.9). The image field of view corresponds to approx. 33 x 25 mm<sup>2</sup>. An offset between reference and object wave is introduced to generate a spatial phase gradient of  $\beta_x = 0.50v_{Ny,x}$ ,  $\beta_y = 0.48v_{Ny,y}$  for spatial phase shifting, where  $v_{Ny,x}$  denotes the horizontal and  $v_{Ny,y}$  the vertical sampling frequency. Reference wave and object beam (before it is reflected from the object's surface) are vertically polarized (normal to the plane containing the beams).

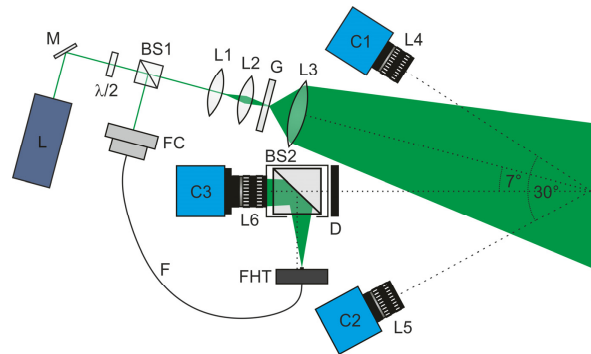


Fig. 6. Top view of the experimental setup of the combined measurement system. BS1: polarizing beam splitter; BS2: beam splitter; C1, C2, C3: CCD cameras; D: diaphragm; F: single-mode fiber; FC: fiber coupler; FHT: fiber holder in translation stage; G: ground glass; L: laser; L1, L2, L3: lenses; L4, L5, L6: C-mount lenses;  $\lambda/2$ : rotatable half-wave plate; M: mirror.

Two additional monochrome CCD cameras (C1, C2; 1280 x 960 pixels, 256 gray levels; DMK 41BF02, The Imaging Source) with 50 mm C-Mount lenses (23FM50SP/23FM50, Tamron) are used to record a stereo image pair of the object. The field of view is 50 x 38 mm<sup>2</sup> in size.

For the investigation of the precision of DHI a white-painted metal beam is tilted, for the investigation of the precision of DSP a plate is translated. Both operations are performed with a piezo motor linear stage (CONEX-AG-LS25-27P, Newport, Irvine, CA, USA). The stage is calibrated prior to the measurement. For this purpose, an array of circular marks is temporarily fixed to the plate. The shift of these marks is acquired by fitting ellipses to the marks in the images from before and after the shift, and calculating the average translation of the centers of these ellipses.

## 2.6 System calibration

For the acquisition of 3D coordinates the system has to be calibrated photogrammetrically. The interior and exterior parameters of all three cameras are retrieved employing the method of Zhang [27,28] using a small plane pattern of circular marks as calibration target.

For precise calculation of the sensitivity vector the positions of the diaphragm and the collimator lens in front of the ground glass have to be determined. This task is also performed photogrammetrically by using a digital single-lens reflex (DSLR) camera (D7000, Nikon, Tokyo, Japan) with a field of view large enough to capture both devices as well as an additional medium-sized calibration target (80 mm x 60 mm). This target is used to determine the exterior parameters of the DSLR in the following photogrammetric measurements of the position of the small calibration target, the diaphragm and the collimator lens in front of the ground glass. In the final calibration step the transformation between the coordinate system of the DSLR measurements and the measurement system is calculated based on the coordinates of the points on the smaller calibration target determined by each method. Using this transformation the location of the diaphragm and the collimator lens in front of the ground glass are gained in the coordinate system of the measurement system.

## 2.7 Software

Software for image acquisition and camera calibration was written in C++ using the Microsoft DirectX programming interface, the free library OpenCV [28] and libraries from The Imaging Source (Bremen, Germany).

For retrieval of 3D shape and deformation from the recorded images another software has been developed. It uses the programming language C# and the free numeric libraries Alglib [29] and fftw [30].

## 2.8 Methods for characterization and optimization of the combined system

It is expected that some of the key parameters of our approach have opposing effects on the performance of the combined techniques. Thus, in a first step each technique is optimized individually. Afterwards, recommended parameter sets for combined measurements are derived.

The quality of data retrieval with DHI is characterized by quantifying the noise of wrapped phase difference distributions modulo  $2\pi$  that are obtained from a vertically tilted white-painted metal beam. Therefore, the standard deviation of the original measured data to low-pass filtered data is calculated [31]. For filtering, the sine and cosine of the phase difference distribution are smoothed separately by successive application of an average filter. For measurements with a fixed tilt of the painted metal beam a kernel size of  $9 \times 3$  pixels is used while for measurements with varying tilts a kernel of  $9 \times 1$  pixels is applied. Each filter is applied 30 times [19].

To characterize the accuracy of the reconstruction of the object wave's intensity distribution the normalized cross correlation between reconstructed and separately recorded intensity distributions is calculated [4].

For performance evaluation of DSP, a glass plate with an attached piece of white paper is translated horizontally with a linear stage. The precision of the measured in-plane displacements is characterized by their standard deviation. Outliers are defined as values smaller than  $Q_1 - 3(IQR)$  or larger than  $Q_3 + 3(IQR)$  and are discarded, where  $Q_1$  and  $Q_3$  are the first and third quartiles of the measured displacements, respectively, and IQR denotes the interquartile range.

The precision of the 3D data acquisition by projection of a speckle pattern is quantified by measuring a 3D printed white-painted spherical surface (radius: 15 mm) and determining the mean distance of the measured data to a reference data set. The reference data is obtained by measuring the shape of the surface using a fringe projection system (Atos, GOM, Braunschweig, Germany). A least squares best-fit is employed to transform both measurements into the same coordinate system.

## 2.9 Determination of mean speckle size

The mean speckle size is defined as the width of the normalized autocorrelation function of the imaged speckle pattern. It is calculated by fitting a two-dimensional Gaussian function to the normalized two-dimensional autocorrelation function and retrieving its average full width at half maximum. The autocorrelation function is determined for an area that is located in the middle of the image and measures 512 x 512 pixels. The size of the projected speckles is given for one of the outer cameras (C1) and an f-number of 2.8. A speckle size of 17.2 pixels (px) corresponds to a speckle size of 23.9 px in the images of the camera used for DHI/DSP, a size of 7.5 px to 9.7 px and a size of 3 px to 2.8 px, for example.

## 3. Results

### 3.1 Optimization of the interferometric unit

First, the influence of the ratio between the mean intensities of the reference and object wave  $I_R/I_O$  on the phase noise and the correlation between the distributions of reconstructed and separately measured object wave intensities is investigated. This is performed with and without a polarizing filter in front of the diaphragm for a tilt resulting in approx. 23 phase difference fringes mod  $2\pi$ , which corresponds to a maximum displacement of approx. 6  $\mu\text{m}$ . The average size of the projected speckles is 3 px and the size of the aperture of the diaphragm corresponds to a diameter of the sideband's circumcircle of  $0.83 v_{Ny,x}$  (abbr. A2 in the further text). In addition, reference measurements without projected speckles, i.e., with homogenous illumination, are made. The intensity ratio is determined by calculating the ratio of the mean gray values of separately recorded images of reference and object wave.

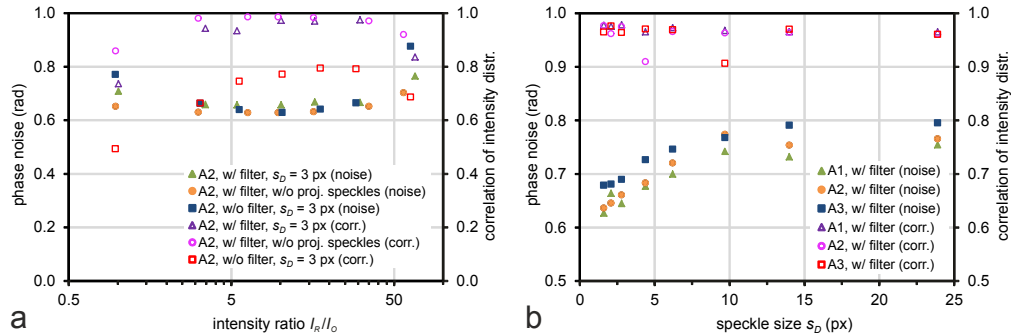


Fig. 7. DHI phase noise and the correlation between the distributions of the reconstructed and separately measured object wave intensities vs. intensity ratio  $I_R/I_O$  (a) and vs. mean size of projected speckles  $s_D$  (b) (for aperture size A1 the diameter of the sideband's circumcircle amounts to  $v_{Ny,x}$ , for A2 to  $0.83 v_{Ny,x}$  and for A3 to  $0.6 v_{Ny,x}$ ).

The results show that intensity ratios from 5:1 to 20:1 ( $I_R/I_O$ ) lead to the lowest phase noise and highest correlation (Fig. 7(a)). While the use of a polarizing filter seems to slightly increase the phase noise in the optimum range of the intensity ratio, it enhances the correlation of the object wave's intensity distribution by 20-50%.

Based on these results, for all further investigations the intensity ratio between reference and object wave is set to approx. 13:1. Figure 7(b) shows the phase noise and the correlation of the intensity distribution of the reconstructed object wave for different aperture sizes and sizes of projected speckles (with polarizing filter, tilt resulting in approx. 23 phase difference fringes mod  $2\pi$ ).

The phase noise increases with increasing size of the projected speckles and decreasing aperture size. On the other hand, the correlation of the intensity distribution is basically independent of these parameters.

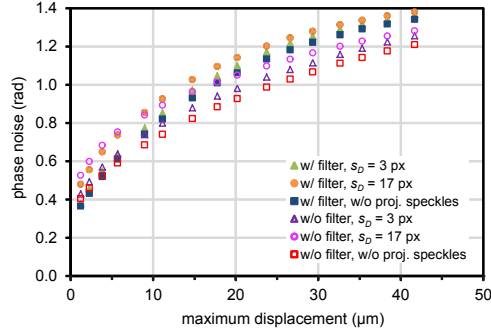


Fig. 8. DHI phase noise in dependency of the magnitude of the maximum displacement resulting from the tilt, the use of a polarizing filter and the size of the projected speckles  $s_D$ .

Next, the measurement range is investigated. To this end, the metal beam is tilted so that maximum displacements between 0 and 42  $\mu\text{m}$  result. Aperture A1 is chosen (the diameter of the sideband's circumcircle amounts to  $v_{N_{y,x}}$ ).

Figure 8 shows that the phase noise increases for increasing displacements. The results indicate that the polarizing filter reduces the noise for small displacements ( $<6 \mu\text{m}$ ). For larger displacements the noise is lower for the configuration without filter. For all configurations, phase noise increases with increasing speckle size. The lowest phase noise for each displacement is obtained without speckle projection.

### 3.2 Optimization of the DSP unit

For the optimization of DSP the standard deviations of the measured displacements for commanded displacements between 1 and 250  $\mu\text{m}$  are determined in dependence on the aperture size and the mean size of the projected speckles. The sub-images measure 64 x 64 px and lie on a regular grid with a spacing of 64 px (391 sub-images per image). A polarizing filter is used.

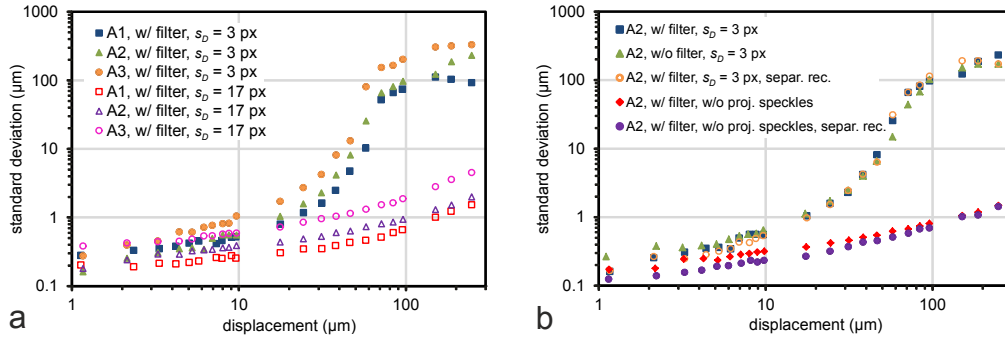


Fig. 9. Standard deviation of the in-plane displacements detected with DSP in dependence on the magnitude of the displacement for different apertures and sizes of projected speckles  $s_D$  (a) as well as for variations of the method (b) (for A1 the diameter of the sideband's circumcircle amounts to  $v_{N_{y,x}}$ , for A2 to  $0.83 v_{N_{y,x}}$ , for A3 to  $0.6 v_{N_{y,x}}$ ).

As can be seen in Fig. 9(a), the measurement range is larger for larger projected speckles. While there are exceptions for displacements smaller than 10  $\mu\text{m}$ , larger apertures result in smaller standard deviations (for a given size of the projected speckles) as do larger projected speckles (for a given aperture size). Noteworthy numbers of outliers ( $>5$ ) (data not shown) usually occur only in measurements whose standard deviations indicate the upper limit of the measurement range for the chosen parameter set.

The polarizing filter as well as recording the object wave's intensity distribution separately instead of reconstructing it from holograms slightly improve the precision but do not extend the measurement range (Fig. 9(b)). Using a homogenous illumination instead of

projecting a speckle pattern leads to higher precision and a larger measurement range (standard deviations less than 2% of the displacement for displacements ranging from 9  $\mu\text{m}$  to 950  $\mu\text{m}$ ) (Fig. 9(b)).

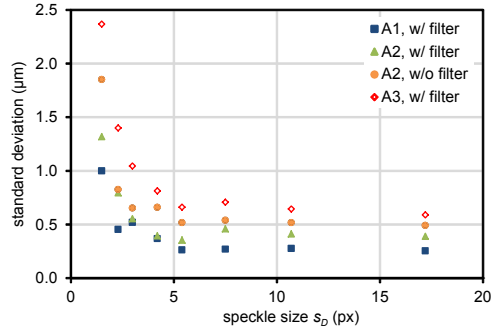


Fig. 10. Standard deviation of the measured in-plane displacement for a horizontal displacement of approx. 10  $\mu\text{m}$  in dependence on the size of the projected speckles and the aperture (for A1 the diameter of the sideband's circumcircle amounts to  $v_{Ny,x}$ , for A2 to  $0.83 v_{Ny,x}$ , for A3 to  $0.6 v_{Ny,x}$ ).

Figure 10 shows the standard deviations for measurements of a displacement of approx. 10  $\mu\text{m}$  for various sizes of the projected speckles and different apertures. The lowest standard deviations are obtained for the largest aperture investigated and projected speckles larger than 5 px. A polarizing filter decreases the standard deviation on average by approx. 20%.

### 3.3 Optimization of the photogrammetric unit

For the optimization of the 3D shape acquisition the influence of the size of the projected speckles and the apertures of the outer cameras (C1, C2) is investigated. In the correlation process a subset size of 33 x 33 px and a grid spacing of 16 px are used. The images are pre-processed using a Gaussian filter with a kernel size of 5 x 5 px. Before filtering, the gray level histograms of the images are equalized [32]. The threshold for the correlation coefficient is set to  $5 \cdot 10^{-5}$ .

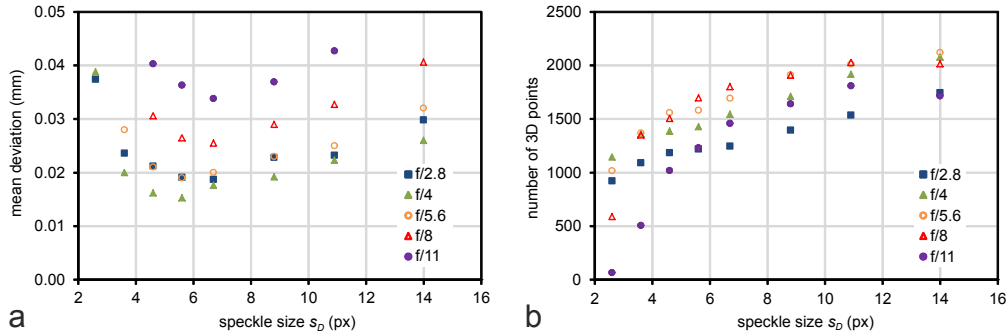


Fig. 11. Mean deviation from 3D reference measurement (a) and number of successfully determined 3D points (b) for different f-numbers and average sizes of the projected speckles.

The results indicate that the lowest deviations from the reference measurement are obtained for average speckle sizes between 5.5 and 7 pixels (Fig. 11(a)). The number of successfully reconstructed 3D points increases with the speckle size (Fig. 11(b)). F-numbers ranging from f/2.8 to f/5.6 yield the lowest mean deviations from the 3D reference measurement, f-numbers from f/4 to f/8 the highest numbers of 3D points.

#### 4. Discussion

The results in sections 3.1 and 3.2 show that the highest performance of DHI and DSP is achieved with homogenous illumination, but using an additional speckle pattern for illumination does not present a major restriction. While larger projected speckles are advantageous for the precision and measurement range of DSP (Fig. 9(a), Fig. 10), they increase phase noise in DHI, where smaller projected speckles are preferable (Fig. 7(b)). Unwrapping of phase difference maps with high fringe densities is observed with less unwrapping error for smaller projected speckles even though the quantity of the phase noise might be higher. Successful unwrapping, however, depends on many factors, e.g., the used phase unwrapping algorithm, fringe density and variations in fringe orientation.

Apparently, the projection of speckles amplifies speckle de-correlation [33]. For DHI this is less critical, as the dimensions of the projected speckles, especially in illumination/viewing direction [17], are typically large compared to the investigated deformations. However, translations in the optimal measurement range of DSP (9-950  $\mu\text{m}$  with homogenous illumination) are at least of the same magnitude as the dimensions of the projected speckles in the measurement plane.

For 3D data acquisition larger projected speckles lead to a more robust correspondence analysis, and thereby to a higher number of successfully reconstructed 3D points (Fig. 11(b)). The highest precision is obtained with speckle sizes between 5.5 and 7 px (Fig. 11(a)). However, this result is most likely only valid for the investigated sub-image size of 33 x 33 px. Further investigations (data not shown) revealed that with 53 x 53 px sub-images the highest precision is obtained for speckles larger than 8 px (the lowest deviations are around 35% higher than with 33 x 33 px sub-images, though). These results confirm qualitatively our previous findings presented and more thoroughly discussed in [8].

In conclusion, for simultaneous measurements the optimum choice of the size of the projected speckles depends on the magnitude and direction of the expected deformations. Table 1 summarizes recommended speckle sizes for different deformation ranges. A speckle size of 10 px corresponds to approx. 0.4 mm in the object plane. These recommendations are not universal and will have to be adapted to the used imaging setup. Note that deformation measurements with the presented 3D data acquisition method are restricted in that the projected pattern is not fixed to the surface of the object under test. For example, a vertical translation of a vertically aligned cylinder cannot be retrieved. Furthermore, with increasing in-plane deformations the DHI phase noise will increase due to speckle de-correlation. The DHI phase noise can be reduced by compensation of the speckle de-correlation by shifting the reconstructed object wave's complex amplitude back based on DSP displacement data [4,33].

**Table 1. Recommended size  $s_D$  for projected speckles<sup>a</sup>**

max. absolute value of in-plane deformation $d_{xy}$ / $\mu\text{m}$	max. absolute value of out-of-plane deformation $d_z$ / $\mu\text{m}$			
	0	$0 < d_z \leq 30$	$30 < d_z \leq 1000$	$> 1000$
0	m/l	none	m/l	m/l
$0 < d_{xy} \leq 10$	none	none	m/l	l
$10 < d_{xy} \leq 950$	none	none	l	l
$> 950$	m	m	m/l	m/l

<sup>a</sup>m: medium ( $5 \text{ px} < s_D \leq 10 \text{ px}$ ); l: large ( $10 \text{ px} < s_D \leq 20 \text{ px}$ ); none: no speckles should be projected and the 3D data acquisition should be performed separately.

The measurement ranges of DSP and DHI can be extended by recording intermediate holograms and summing up the determined deformations [34]. This way a possible gap to the optimum measurement range of the photogrammetric method could be closed if the measurement conditions allow the recording of additional images.

The results in Fig. 7(b) and Fig. 10 show that the aperture of the diaphragm in front of the camera used for DHI and DSP (C3) should be as large as possible. A larger aperture causes smaller subjective speckles, shorter exposure times and a smaller depth of field. The latter is of minor significance for the investigations described in section 3.1 and 3.2 as only flat objects aligned nearly parallel to the image plane were tilted and shifted. For less parallel surfaces the smaller depth of field will likely reduce the precision in areas not in focus.

Smaller exposure times allow a faster data acquisition and lead to less image noise, which benefits the precision of DHI and DSP. Smaller subjective speckles result in an increased spatial resolution. In DSP smaller subjective speckles mean that the subsets contain more information in form of gray value variations and might allow more precise calculations. The upper limit of the aperture size is given by the fact that for the FTM to work properly the sidebands in the spectrum must not overlap each other. In addition, the subjective speckles must be large enough to be resolvable by the camera sensor.

The intensity ratio between reference wave and object wave influences the exposure time and is also reflected in the spatial frequency distribution of the hologram. The lower  $I_R/I_O$ , the higher is the relative intensity of the speckle halo in the frequency domain and the more considerable is its overlap with the sidebands. This results in a higher demand for its removal from the spectrum. For a fixed overall intensity a lower ratio  $I_R/I_O$  also means longer exposure times (hence, more noise), as in practice almost the entire laser light is used for object illumination and  $I_O$  is hence almost solely controlled by the exposure time. On the other hand, the modulation decreases and the influence of quantization errors increases for increasing  $I_R/I_O$ . Intensity ratios from 5:1 to 20:1 appear to be the best compromise (Fig. 7(a)).

A polarizing filter incorporated into the observation path eliminates light with an improper polarization. While the polarization filter clearly leads to a more accurate reconstruction of the object wave's intensity distribution (Fig. 7(a)) and higher precision in DSP (Fig. 10), it does not improve the performance for the detection of optical path length changes with DHI (Fig. 8). Apparently, errors in the reconstruction introduced by mismatching polarization are compensated by the subtraction of the two phase maps modulo  $2\pi$ . Phase differences maps obtained without the polarizing filter actually appear slightly improved with respect to phase noise (Fig. 8). A comparative measurement using a neutral density filter instead of the polarizing filter indicates that this is not caused by increased exposure times due to the lower intensity of the object wave resulting from light absorption. The reason for this behavior remains unclear. Accordingly, the polarizing filter should not be used if primarily out-of-plane deformations are to be measured (especially since the use of the filter increases the measurement time).

From the results in Fig. 11 it can be concluded that for the 3D data acquisition apertures with f-numbers  $f/4$  or  $f/5.6$  can be regarded as the best compromise considering the number of found correspondences and their accuracy. On the one hand, a larger aperture results in less image noise (due to shorter exposure times) and smaller subjective speckles. Subjective speckles have to be considered noise in this context, as they differ for both cameras, thus interfering with the correlation process, which aims to find similar structures of objective speckles. On the other hand, a larger aperture reduces the depth of field and hence the area that can be evaluated.

The reconstruction of the object wave's intensity distribution from the hologram proves to be highly accurate (Fig. 7(b)). Consequently, this reconstructed intensity distribution could more than likely replace the image of camera C1 or C2 in 3D shape acquisition, rendering one of these cameras unnecessary.

## 5. Application examples

To demonstrate the applicability of our approach, first the three-dimensional deformation of a mandible model due to mechanical loading of an inserted dental implant is determined. The model measures 70 x 36 x 30 mm (W x D x H) and consists of rigid polymer. It was fabricated using a 3D printer and spray-coated with laser scanning spray. The implant (diameter: 2.5 mm, length: 9 mm) is made of titanium and provided with a ball abutment. Using a force gauge a load of 20 N is applied to the top of the implant. For 3D shape acquisition speckles with a diameter of 14 px are projected and a sub-image size of 53 x 53 px is used (aperture:  $f/4$ ; grid spacing: 16 px). Although very small deformations are expected, the DHI-DSP measurement is carried out simultaneously for demonstration (aperture: A1; without polarizing filter; sub-image size: 64 x 64 px; grid spacing: 64 px).

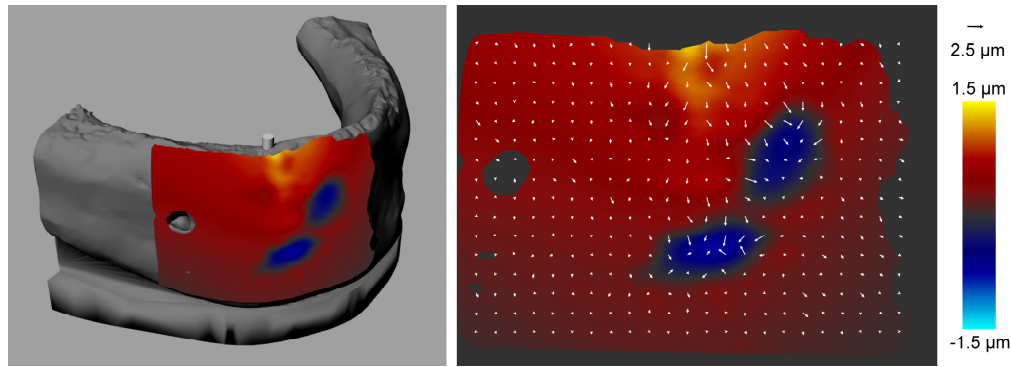


Fig. 12. Out-of-plane deformation mapped onto measured surface (full model of mandible (gray) shown for illustrative purposes only) (left) and 3D deformation (right). Pseudo-colors are used to represent the out-of-plane component of the deformation, arrows (length scaled up by a factor of 200) indicate the in-plane components.

The obtained results are depicted in Fig. 12. It shows the acquired surface in pseudo-colors according to the measured out-of-plane deformation and arrows indicating the in-plane deformation. In addition, the entire 3D model of the mandible (as it was constructed) and a cylinder indicating the position of the implant are shown. The 3D model has been transformed into the coordinate system of the measurement system by a least squares best-fit to the measured surface data. Although the observed in-plane deformations are below the optimum measurement range of the setup, the presented approach proves to be feasible.

In the second application example, the shrinkage of dental impression material (alginate) is observed. The alginate is filled into a metal impression tray. A spherical impression is formed by pushing a steel ball (diameter: 8 mm) into the alginate. For 3D shape acquisition speckles with a diameter of 7.5 px are projected. As the alginate is partly translucent, the projected speckles appear blurred and approx. three times larger. Hence, a large sub-image size of 83 x 83 px is chosen (aperture:  $f/4$ ; grid spacing: 16 px). DHI measurements are carried out simultaneously (aperture: A1; without polarizing filter). The measurement starts 80 minutes after the impression has been made.

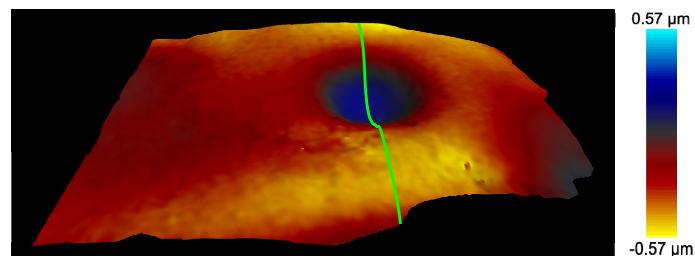


Fig. 13. Out-of-plane deformation after 20 s mapped onto measured surface. The green line indicates the position of the sections shown in Fig. 14.

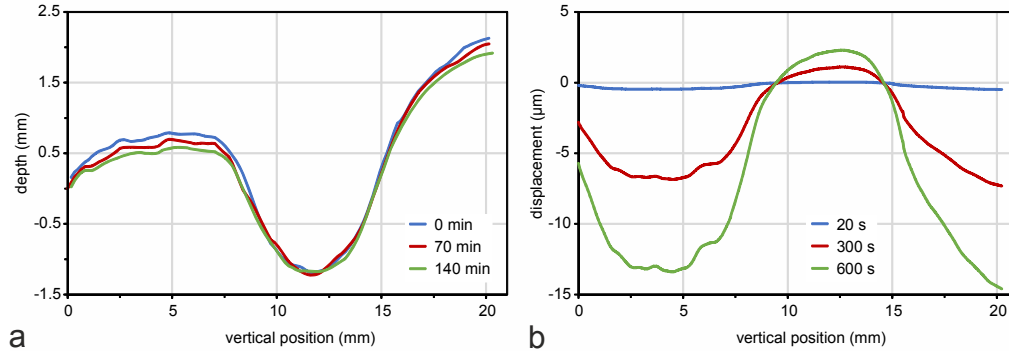


Fig. 14. Sections through the surfaces determined with 3D shape acquisition after different time periods (0 min, 70 min, 140 min) (a) and through the out-of-plane displacement maps determined with DHI after different time periods (20 s, 300 s, 600 s) (b).

Figure 13 and Fig. 14 depict the results. The measured deformations are shown relative to a point near the edge of the tray. Changes in the microstructure of the surface led to strong decorrelation before the upper limit of the measurement range of DHI was reached. Hence, deformations between successive hologram recordings (time interval: 20 s) were calculated and summed up. The results show that despite the challenging surface/material properties of the drying up alginate, quantitative measurements of the shrinkage are possible.

## 6. Conclusions

A measurement system combining Digital Holographic Interferometry (DHI), Digital Speckle Photography (DSP) and photogrammetry based on digital image correlation of a projected laser speckle pattern has been presented. The influence of key parameters like the intensity ratio between object and reference wave as well as the sizes of the projected speckles and apertures on precision and measurement range was characterized. Our results show that DHI and DSP can be applied in combination with a projected speckle pattern for the simultaneous acquisition of macroscopic 3D shape data. This is especially useful for the observation of fast 3D deformations where short measurement times are crucial. As the size of the projected speckles had shown an opposing effect on the performance of DHI and DSP, recommendations for the choice of this parameter with regard to the expected deformations were provided.

Despite some constraints (reduced spatial resolution, no tracking of specific surface points), the photogrammetric method provides a useful tool to extend the measurement range of DSP and DHI. Other advantages of the presented approach are the more accurate calculation of the sensitivity vector and the option to precisely assign measured deformations to the macroscopic shape of the investigated object/specimen. This allows an improved visualization of the observed deformations, which was demonstrated in the measurement of the deformation of a mandible model due to mechanical loading of an inserted dental implant and the monitoring of the shrinkage of dental impression material. Furthermore, it can be used to compare measured deformations with data from numerical simulations, e.g., finite element analyses.

In comparison to previous approaches that combine measurements of microscopic 3D deformations and macroscopic shape acquisition [6], the proposed experimental setup is rather simple. It could be further simplified by eliminating one of the cameras used for the 3D shape measurement. Instead, the object wave's intensity distribution reconstructed from a hologram could be used.

## Acknowledgments

We acknowledge support by Open Access Publication Fund of University of Muenster.